Carbon 155 (2019) 570–579

Contents lists available at ScienceDirect

Carbon

journal homepage: www.elsevier.com/locate/carbon

Template dissolution with NaOH–HCl in the synthesis of zeolite-templated carbons: Effects on oxygen functionalization and electrical energy storage characteristics

Hongjun Park [a, b], Steven K. Terhorst [b, 1], Raj Kumar Bera [b], Ryong Ryoo [b, a, *]

[a] Department of Chemistry, Korea Advanced Institute of Science and Technology (KAIST), Daejeon, 34141, Republic of Korea
[b] Center for Nanomaterials and Chemical Reactions, Institute for Basic Science (IBS), Daejeon, 34141, Republic of Korea

ARTICLE INFO

Article history:
Received 10 July 2019
Received in revised form
27 August 2019
Accepted 6 September 2019
Available online 6 September 2019

ABSTRACT

Zeolite-templated synthesis is a versatile route to ordered microporous carbons built with single-walled sp^2 framework of various structures, but the use of hazardous HF to dissolve the zeolite template is still a critical safety issue. We investigated the template-removal process using NaOH and HCl, which are safer than HF. The results indicated that the residual ash content in the carbon could be lowered to less than 5 wt% when the template was removed by consecutive treatments using NaOH and HCl in a proper sequence depending on the zeolite framework type. The carbon obtained in this manner exhibited a rather increased supercapacitance in aqueous media at high current density, as compared to carbons from HF-washing. In the case of the non-aqueous supercapacitor, however, the washing with NaOH–HCl resulted in low capacitance. This was due to the effect of NaOH to generate oxygen-functional groups, which could lead to an increase in the hydrophilicity, and a decrease in the electrical conductivity. Furthermore, the oxygen-functional groups could serve as a base to graft organic amines. When the carbon was heated in H_2, the oxygen content decreased to a similar level to that of the HF-washed carbon, restoring the conductivity and electrochemical energy storage characteristics.

1. Introduction

Zeolites are a family of crystalline microporous aluminosilicate minerals with various framework types possessing different pore shapes, connectivity and diameters [1]. Some of the zeolite types, such as FAU, EMT and beta [2], have pore diameters similar to the diameter of C_{60} fullerene and nanotube derivatives [1]. For this reason, zeolites have been investigated for a long time as a template for the synthesis of three-dimensionally (3D) periodic nanostructures built with single-layered sp^2 carbon frameworks [3–8]. The zeolite-templated synthesis is performed by deposition of carbon inside the zeolite pores via pyrolytic carbonization of organic compounds [8]. The deposited carbon is then released from the template through the dissolution of the aluminosilicate zeolite framework.

The template dissolution in synthesis of zeolite-templated carbon (ZTC) thus far has been performed mostly using HF [5–10]. HF is the most effective reagent to dissolve aluminosilicate zeolite, but its toxicity brings a critical safety issue. Exposure to HF can cause serious injuries such as severe burns, systemic fluorosis,and even death [11]. To avoid the safety hazards arising from HF, NaOH has been considered as an alternative reagent to wash off the zeolite from a zeolite/carbon composite. Ryoo et al. addressed that the zeolite template could be dissolved by NaOH and HCl solutions in the case of beta zeolite [12,13]. Indeed, the NaOH-based dissolution can be effective for such a high-silica zeolite consisting of more than 90 wt% of SiO_2. However, when the aluminum content of the template is exceedingly high as in the case of FAU (X and Y) type, zeolite dissolution by NaOH becomes difficult. This is because of the chemical resistance of Al–O–Si covalent bonds in the zeolite framework [14]. Recently, Moon et al. reported the removal of Y zeolite template by washing twice with 2 M NaOH solutions, and subsequently once with 0.1 M HCl [15]. When this procedure was followed in our laboratory, the resultant ZTC product contained 14 wt% of non-carbonaceous inorganic residue (see Entry 7 in

* Corresponding author. Center for Nanomaterials and Chemical Reactions, IBS, Daejeon, 34141, Republic of Korea.
E-mail address: rryoo@kaist.ac.kr (R. Ryoo).
[1] Current address: Institute of Organic Chemistry, Landoltweg 1, Aachen 52,062, Germany.

https://doi.org/10.1016/j.carbon.2019.09.020
0008-6223/

Table 1).

In an attempt to remove the zeolite template more effectively using NaOH and HCl solutions, we reinvestigated the dissolution of X, Y and beta zeolites. The zeolite dissolution was investigated under various conditions, including reagent concentration, treatment temperature, and sequence of NaOH and HCl treatments. Based on the result, the template-dissolution process was optimized with respect to the individual zeolites with various silicon to aluminum (Si/Al) ratios. In the course of the present study, we discovered that the oxygen content in ZTC increased significantly due to the NaOH treatment. Consequently, the changes of the oxygen content markedly affected the electrical conductivity and energy storage performance of the carbons in supercapacitor applications. The oxygen content of the carbons decreased when the ZTC was heated with H_2. In this paper, we report comprehensive results, including the zeolite-dissolution conditions, the resultant oxygen content in ZTC, electrical conductivity, electrochemical energy storage characteristics, and the effect of the H_2 treatment. Moreover, we utilized the oxygen functionality as an anchoring site for an organic amine group and evaluated its catalytic activity in Knoevenagel condensation.

2. Experimental section

2.1. Carbon deposition and zeolite dissolution

Beta zeolite (HSZ-931HOA, Si/Al = 14) was purchased in a powder form from Tosoh, and X zeolite (13X, Si/Al = 1.2) from Sigma-Aldrich. Y zeolite (Si/Al = 2.4) was prepared, following the same procedure as previously reported [16]. The zeolites were ion-exchanged to a Ca^{2+} form prior to carbon deposition, according to the carbon synthesis procedure reported in our recent work (see Section 1.1 for Materials and Methods in Supplementary data) [17]. The zeolite pores were then filled with carbon via pyrolytic carbonization of ethylene at 873 K, following the procedure using 0.5–30 g of zeolite [17]. In a typical synthesis, zeolite was loaded in a vertical quartz tube reactor ($d = 15$ mm), which was equipped with a quartz fritted disc. The reactor was heated to 873 K at a ramping rate of 5 K min^{-1} under dry N_2 flow and maintained at this temperature. Then, the N_2 flow was combined with ethylene gas and switched to pass through a water bubbler. The temperature of the bubbler was kept at 303 K. The N_2/C_2H_4 ratio was 4:1 in volume ratio, and the total flow rate was 78 cm^3 min^{-1}. The gas flow was continued for 4 h and switched back to dry N_2. The zeolite/carbon composites were subsequently heated at 1123 K for 1.5 h. Removal of the zeolite template from the resultant zeolite/carbon composite was tested in a NaOH, HCl, or HF solution. The test was performed in a single step, or in a sequence using different solutions under stirring. In the case of NaOH, the NaOH concentration was selected as 0.1 or 2 M in a 1:1 water-ethanol mixture (in volume ratio), depending on the zeolite type. The amount of the NaOH solution was 40 mL per 0.5 g of zeolite/carbon composite. After stirring in a polypropylene bottle (typically, for 2 h unless specified otherwise), the solid residue was collected by vacuum filtration (or centrifugation), and dried in an oven at 373 K after washing with doubly-distilled water. In the case of HCl or HF, the treatment was performed with an aqueous solution of 0.1 M HCl, 1 M HCl, 3 M HCl, or a 1 M HF-1 M HCl mixture.

2.2. Post-synthetic H_2 treatment of carbons

Typically, 0.1 g of carbon was placed in a lab-made glass reactor and evacuated for 1 h under a vacuum. The reactor was subsequently heated at 723 K (ramping rate: 5 K min^{-1}) for 2 h under H_2 gas flow of 60 cm^3 min^{-1}.

2.3. Materials characterization

Materials characterization was performed with thermogravimetric analysis (TGA), X-ray powder diffraction (XRD, X-ray wavelength of 0.154 nm), scanning electron microscopy (SEM), energy dispersive X-ray spectroscopy (EDS) transmission electron microscopy (TEM), argon adsorption at 87 K, elemental analysis, ^{13}C magic angle spinning nuclear magnetic resonance (MAS NMR), attenuated total reflectance-Fourier transform infrared (ATR-FTIR), four-point probe method, and conductive atomic force microscopy (C-AFM). Solid-state ^{13}C NMR spectroscopy was performed using a NMR spectrometer (Bruker AVANCE III HD 400WB). The spectrometer was equipped with a 4 mm MAS probe, and the sample in a zirconia rotor was spun at 13 kHz. The ^{13}C frequency was 100.63 MHz and the $\pi/2$ pulse width was 4 μs. ^{13}C cross-polarization (CP) MAS NMR measurement was conducted with a contact time of 2 ms. The chemical shift was calibrated using adamantane. ATR-FTIR spectra were recorded on an FTIR spectrometer (Thermo Scientific Nicolet iS50), equipped with a diamond ATR window. C-AFM was carried out with an atomic force microscope (Bruker Multimode 8). Sheet resistances were measured with a four-terminal sensor (Signatone SP4) by the four-point probe method [18]. Current-voltage (I–V) curves were obtained using a doped-diamond-coated probe (DDESP-V2, Bruker) at a bias voltage of 1 V. The remaining characterization procedures were the same as described elsewhere [17].

2.4. Electrochemical measurement

The specific capacitance was measured in a two-electrode cell, either in a non-aqueous medium of 1 M tetraethylammonium tetrafluoroborate/propylene carbonate (Et_4NBF_4/PC), or in a 1 M K_2SO_4 aqueous solution. For the non-aqueous supercapacitor, the working electrodes were prepared by following the procedure in the literature [12]. In brief, Super P was used as a conductive agent. Polyvinylidene fluoride (PVDF) was the binder. ZTC, Super P and PVDF powder samples were homogeneously mixed in an *N*-methyl-2-pyrrolidone solution to prepare a carbon ink. The ZTC/Super P/PVDF ratios were 8/1/1 in weight. The slurry, which was obtained from the mixture, was uniformly coated on an Al foil ($t = 30$ μm) and dried at 383 K for 4 h under vacuum. The dried film was punched out to make a circular working electrode ($d = 12$ mm). The mass loading of ZTC in the working electrode was 2.0 mg cm^{-2}. Cyclic voltammetry (CV) and electrochemical impedance spectroscopy (EIS) measurements were performed at 298 K using a workstation (Autolab PGSTAT30). The CV curve was obtained by repetitive scans for stabilization. Afterward, the galvanostatic charge/discharge (GCD) profile was recorded with a current density range of 0.1–10 A g^{-1} on a battery cycler (WonATech WBCS3000) at 298 K. The voltage window for the non-aqueous supercapacitor was 0–2.5 V.

For an aqueous supercapacitor, a carbon ink was prepared by dispersing 10 mg of ZTC in a mixture of 0.2 mL of water, 0.05 mL of 5 wt% Nafion, and 0.75 mL of ethanol by sonication for 1 h. The working electrode was prepared via drop casting 100 μL of the ink on a circle shape carbon cloth ($d = 15$ mm). The mass loading of ZTC in the working electrode was 1.0 mg cm^{-2}. The voltage window for the aqueous supercapacitor was 0–0.9 V.

The specific capacitance was calculated from the GCD curve by following the calculation method in the literature: $C_s = 2 \times I \times \Delta t / \Delta V \times m$, where I is the constant discharging current, Δt is the discharging time, ΔV is the discharging voltage, and m is the mass of active material on one electrode [19]. The current density was the current divided by a single-electrode mass.

3. Results and discussion

3.1. Removal of zeolite templates by NaOH and HCl

The zeolite template has various Si/Al ratios from 1 to infinity according to the structure type [1]. Depending on the zeolite Si/Al ratio, the zeolite framework is built with different proportions of Si–O–Si and Al–O–Si covalent bonds [20]. The Si–O–Si bonds can be relatively easily hydrolyzed in an aqueous solution of NaOH [21]. On the other hand, the Al–O–Si bonds show high chemical resistance to NaOH [22]. The framework Al in the bond can alternatively be leached out with HCl [23]. In this regard, NaOH is often used for desilication of zeolites, while HCl is employed for dealumination. Upon the desilication or dealumination processes, structural defects are formed in the zeolite, which destabilizes the aluminosilicate framework [14]. Hence, after the desilication by NaOH or dealumination by HCl, the remainders of the zeolite can be more easily dissolved when treated with the other solution. Based on the dissolution characteristics, we tested the zeolite template-removal procedures using NaOH and HCl solutions either singly or consecutively in different orders. The dissolution results obtained in this manner are summarized in Table 1.

As shown in Table 1, when beta zeolite with Si/Al = 14 was used as a template for ZTC, the template washing at 353 K with a 2 M NaOH solution was able to remove 96% of the initial zeolite content. Because the beta zeolite had a high silica content (>93%), the zeolite structure could be destroyed by a single treatment with NaOH [21]. The NaOH-washed product had a non-carbonaceous ash content of 9.8 wt%, as measured by TGA (Entry 1 in Table 1), which was mostly amorphous aluminosilicate. On the other hand, the washing treatment with a 1 M HCl solution at room temperature (rt) failed to dissolve the beta zeolite due to its low Al content, retaining the zeolite content in the pristine zeolite/carbon composite (Entry 2). Increasing the HCl concentration to 3 M was also unable to dissolve the beta zeolite. The 1 M HCl followed by the 2 M NaOH treatment (*i.e.*, rt 1 M HCl/353 K 2 M NaOH, Entry 3) gave a product with similar ash content (7.3 wt%) to the result using only NaOH, which suggested that the initial HCl treatment was not effective for dissolving the beta template. In contrast, the 2 M NaOH followed by the 1 M HCl treatment (Entry 4), lowered the ash content to 2.0 wt %. This result indicates that it was easier to remove the residual aluminous species after destroying the highly siliceous zeolite structure with NaOH. The resultant ash content (2.0 wt%) was higher than that from the result of HF–HCl treatment (0.5 wt%). The 2.0 wt% ash consisted of amorphous aluminosilicates with Si/Al = 107, as determined by EDS. We tried to further decrease the ash content through one more NaOH treatment, but the treatment caused a significant damage to the structure of the carbon (Fig. S1). For this reason, we believed that the '353 K 2 M NaOH/rt 1 M HCl' washing (Entry 4) was the optimal method among the four conditions tested for washing off the beta template (Entries 1–4).

Although the '353 K 2 M NaOH/rt 1 M HCl' treatment was effective for the removal of beta zeolite template, the method resulted in a high ash content of 13.3 wt% when applied to the Y zeolite template (Table S1). This result was reasonable considering the high Al content (*i.e.*, low Si/Al of 2.4) of Y zeolite. The Y zeolite framework has a high proportion of Al–O–Si bonds, which have resistance to the attack by both NaOH and HCl [24,25]. Considering the high Al content, we added a 1 M HCl treatment prior to the '353 K 2 M NaOH/rt 1 M HCl' treatment. The ash content then decreased to 4.3 wt%, indicating that 99% of the initial zeolite was removed. The ash content of 4.3 wt% was in a form of amorphous aluminosilicates (Si/Al = 24). This result implied that the initial HCl treatment could effectively destabilize the Y zeolite framework, thereby facilitating the subsequent silica dissolution by NaOH [24]. Moreover, the HCl concentration of 1 M was sufficient for the template washing. An increase of the HCl concentration to 3 M did not change the resultant ash content significantly, as in the case of beta template removal.

In the case of the ZTC synthesis using X zeolite (Si/Al = 1.2), the template framework could satisfactorily be removed through consecutive treatments of 'rt 1 M HCl/353 K 0.1 M NaOH/rt 1 M HCl' (5.0 wt% of ash, Entry 9). This process was the same as the procedure optimized for the dissolution of theY zeolite template, except that the concentration of NaOH was lowered from 2 to 0.1 M. When 2 M NaOH solution was used, the ash content decreased to 4.4 wt% (Table S1), similar to the case of Y zeolite (4.3 wt% of ash). However, the resultant ZTC product completely lost the micropore order as shown in the XRD pattern (Fig. S2), indicating that severe damages occurred in the carbon framework during the washing

Table 1
Zeolite dissolution effects of NaOH, HCl, or HF.

Entry	Zeolite-Si/Al	Carbon amount[a] (g $g_{zeolite}^{-1}$)	Washing treatment[b]	Ash[h] (wt%)	Carbonaceous (wt %)			S_{BET}[i] ($m^2\ g^{-1}$)	V_{Micro}[j] ($cm^3\ g^{-1}$)
					C	H	O		
1	beta-14	0.33	353 K 2 M NaOH	9.8					
2			rt 1 M HCl	73					
3			rt 1 M HCl/353 K 2 M NaOH	7.3					
4			**353 K 2 M NaOH/rt 1 M HCl**[c]	**2.0**	**90.6**	**1.9**	**7.5**	**3,050**	**1.21**
5			rt 1 M HF-1 M HCl mix[d]	0.5	93.9	2.3	3.6	3,400	1.36
6	Y-2.4	0.33	**rt 1 M HCl/353 K 2 M NaOH/rt 1 M HCl**[e]	**4.3**	**86.6**	**2.6**	**10.9**	**2,000**	**0.81**
7			353 K 2 M NaOH/rt 0.1 M HCl[f]	14	83.0	2.6	14.4	1,580	0.65
8			rt 1 M HF-1 M HCl mix	0.3	94.5	1.5	3.7	2,670	1.07
9	X-1.2	0.32	**rt 1M HCl/rt 0.1M NaOH/rt 1M HCl**[g]	**5.0**	**91.5**	**1.5**	**7.0**	**2,050**	**0.81**
10			rt 1 M HF-1 M HCl mix	0.8	94.5	1.5	3.5	2,560	1.00

[a] The carbon yield was determined by TGA of zeolite/carbon composite samples.
[b] The period of each washing treatment was 2 h at room temperature (rt, 298 K) unless specified otherwise.
[c] The beta template was washed by treating twice with a 2 M NaOH solution for 2 h at 353 K (see Experimental section for each procedure), followed by treatment with a 1 M HCl solution for 2 h at 298 K.
[d] The template was washed twice with a mixture of 1 M HF and 1 M HCl solutions.
[e] The Y template was washed with 1 M HCl, followed by treating twice with a 2 M NaOH solution for 2 h at 353 K. The HCl treatment was repeated once again.
[f] The Y zeolite/carbon composite was treated by following the washing method in Ref. [15].
[g] The X template was washed twice with 1 M HCl, followed by a single treatment with a 0.1 M NaOH solution for 8 h at 298 K. The HCl treatment was repeated once again.
[h] The ash content was determined by TGA of carbon samples at 973 K.
[i] Brunauer-Emmett-Teller (BET) surface area was calculated in a range of $P/P_0 = 0.05–0.15$.
[j] Micropore volume was obtained by quenched solid density functional theory (QSDFT) method.

treatment with 2 M NaOH. From this result, it appeared that the Y zeolite template gave a more chemically robust porous carbon framework against NaOH than that from X zeolite. Another notable point was that the X zeolite framework was easily dealuminated by the initial treatment with 1 M HCl [26], and thus the 0.1 M concentration of NaOH was sufficient in the following treatment.

In summary, the dissolution processes using NaOH and HCl solutions were effective for the removal of zeolite templates from carbon. The resultant ZTC products from beta, Y and X zeolites had an incombustible ash content lower than 5 wt% (Entries 4, 6, 9). The ash content was higher than that of carbons washed with a mixture of 1 M HF and 1 M HCl (Entries 5, 8, 10). The ZTC products washed with NaOH and HCl solutions exhibited a BET surface area greater than 2,000 $m^2 g^{-1}$. Details of the porous texture and chemical properties are provided in the following sections.

3.2. Structure of ZTC from NaOH–HCl

Fig. 1 shows the XRD patterns of the ZTC products obtained by the optimized zeolite-dissolution procedures using NaOH and HCl solutions annotated in Table 1. Bragg peaks were found at diffraction angles between $2\theta = 5–10°$ in each case, representing the zeolite-inherited pore orders in the carbon structure [10,17,27]. However, there were no Bragg reflections corresponding to crystalline zeolite structures. This result indicates complete breakdown of the crystalline zeolite structures by the NaOH–HCl washing processes.

Fig. 2 provides representative TEM and SEM images of the ZTC products. The TEM images exhibited regular lattice fringes, indicating periodically ordered pore network of the carbons. The structural ordering was also presented in the fast Fourier transform (FFT) patterns (insets in Fig. 2). The lattice spacing values from the FFT patterns were well matched with those from XRD patterns (*i.e.*, $d = 1.1$ nm for beta-ZTC and $d = 1.4$ nm for Y-ZTC and X-ZTC), confirming the successful replication of the pore system of the zeolite templates [13]. The SEM images showed that the crystal morphology of the zeolites was well retained in the carbon products even after they were thoroughly washed with NaOH–HCl solutions.

The porous texture of the NaOH–HCl-washed ZTC products was analyzed by Ar adsorption, and compared to that of the carbon products washed with HF (Fig. 3). As shown in the insets in Fig. 3, the Ar adsorption isotherms exhibited a very sharp increase in the adsorption amount (*i.e.*, type-I isotherm) at a relative pressure region below $P/P_0 = 0.02$, indicating that the carbons were highly microporous. The Ar adsorption capacity of the NaOH–HCl-washed carbons was approximately 20% smaller than that of the HF-washed carbons. The decrease in the Ar adsorption capacity correspondingly resulted in lowered BET surface area and micropore volume of the carbons (Table 1). This loss of porosity can be attributed to pore blocking by the ash residues and minor structural damage after the NaOH–HCl washing. Nonetheless, the BET surface area of the beta-ZTC was as high as 3,050 $m^2 g^{-1}$, and it was roughly 2,000 $m^2 g^{-1}$ for both Y-ZTC and X-ZTC. The pore size distributions, derived by the QSDFT method, showed sharp characteristic peaks at around 1 nm in all the carbon samples, which agreed well with the lattice spacing information. This result implies that the pore structure of the carbons was well maintained despite their decreased adsorption capacity after the NaOH–HCl washing treatments.

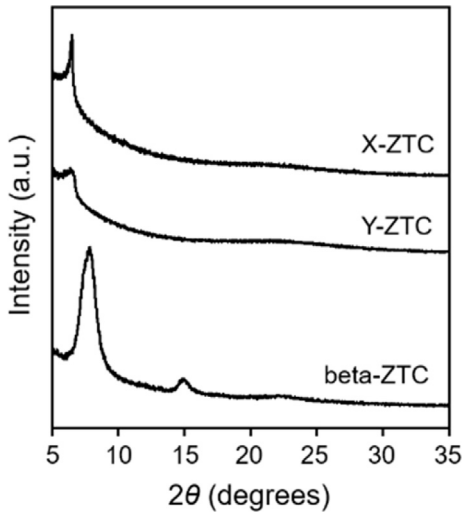

Fig. 1. XRD patterns of beta-ZTC, Y-ZTC, and X-ZTC samples obtained by washing with NaOH and HCl solutions (Entires 4, 6, 9 in Table 1).

3.3. Oxygen functionalization due to NaOH

When washed with the NaOH–HCl solutions, the resultant ZTC products showed an increase in the oxygen content by a factor of approximately two, as compared with the HF-washed carbons (Table 1). To investigate the cause of this phenomenon, we treated a HF-washed beta-ZTC sample in a 2 M NaOH solution at room temperature under stirring for 2 h. Similarly, beta-ZTC-HF was treated in a 1 M HCl solution. The NaOH treatment resulted in a distinct increase of the oxygen content in the carbon from 3.6 to 9.2 wt%, but the HCl treatment caused no significant changes. Moreover, XRD and BET surface area analyses indicated a considerable loss of structural order by the NaOH treatment, whereas the HCl-treated ZTC retained most of the original microporous structure (Fig. S3). As this result shows, the carbon treatment in NaOH solution was the cause of the change in the oxygen concentration.

It has been reported that oxygen-containing functional groups can be generated by a NaOH treatment in the case of activated carbons and carbon black [28–30]. The amorphous carbons such as activated carbons and carbon black are known to contain a significant portion of sp^3 carbons [31], where the formation of oxygen-functional groups is attributed to the surface reaction of NaOH with ether and lactone groups. The increased oxygen content, caused by NaOH, could thus be ascribed to the formation of hydroxyl or carboxyl groups by hydrolysis of the ether and lactone groups [28,29]. Unlike the amorphous carbons, the ZTC is built with mainly sp^2 carbon frameworks, similar to the case of graphenes [13,17]. Many previous works reported that graphenic carbon materials composed of a sp^2 framework did not exhibit a notable increase in oxygen content upon treatments with NaOH solution [32,33]. We ascribed the discrepancy among the sp^2 carbon materials to the strain in the 3D curved graphene structure of ZTC, which was formed inside the nanopores of the zeolite. The ZTC had a tendency to release such strain during the template-dissolution process by hydrolysis of the carbon framework. Nevertheless, it is still unclear how the NaOH treatment could cause the generation of oxygen content on the ZTC surfaces, and further studies are required to understand this phenomenon.

Oxygenation is an important route to functionalization of carbons to increase the hydrophilic property and to graft organic functionalities. In the case of porous carbons, the oxygen functionalization is usually performed with mild oxidizing agents, such as nitric acid, sulfuric acid, or peroxides. A drawback of the oxidative treatment is degradation of the porous structure while the carbon framework undergoes oxidation [34,35]. The structural damage is particularly severe when the pore walls are built with

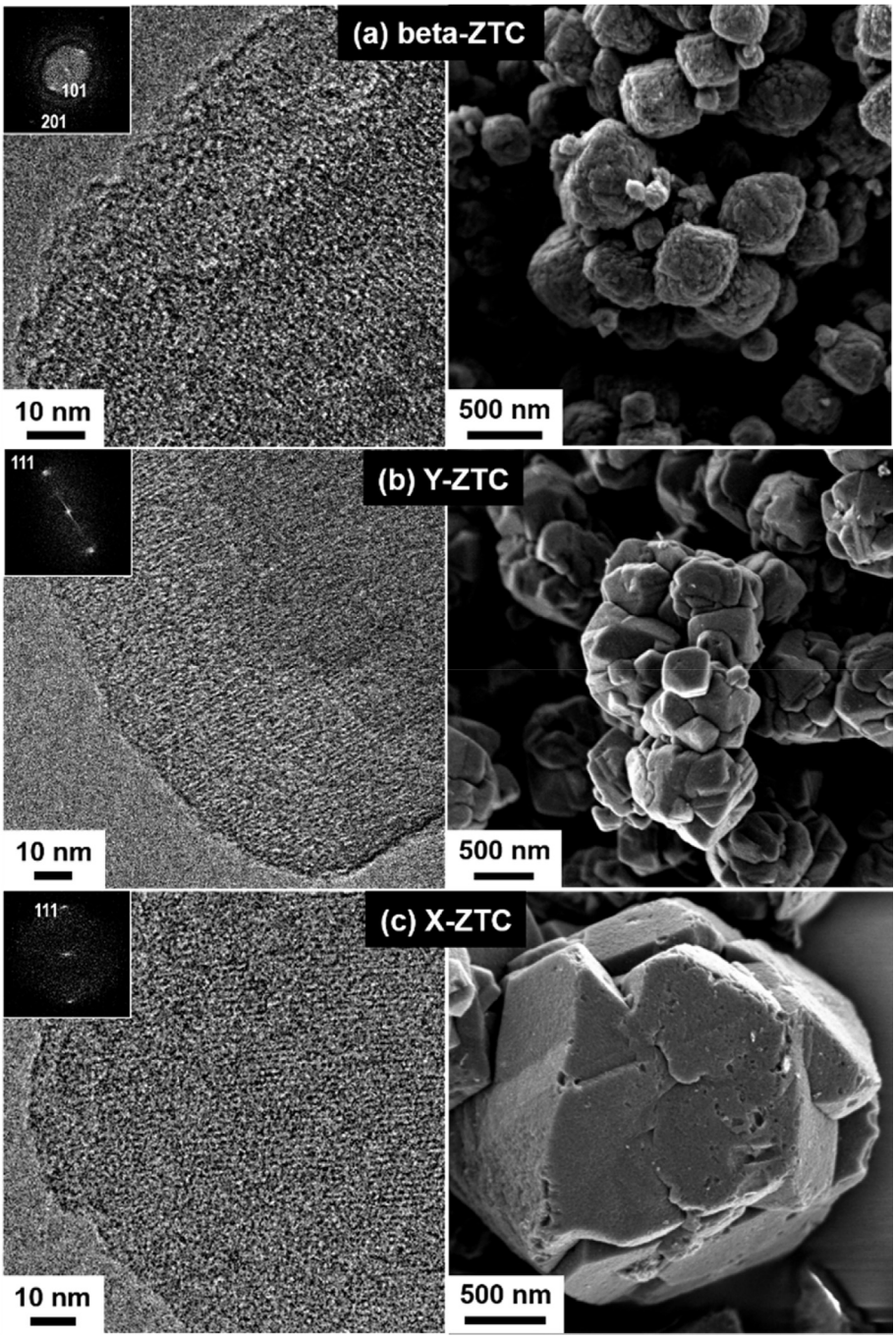

Fig. 2. TEM (left column) and SEM (right column) images of (a) beta-ZTC, (b) Y-ZTC, and (c) X-ZTC samples obtained by washing with NaOH and HCl solutions (Entires 4, 6, 9 in Table 1). Insets in the left column are corresponding Fourier diffractograms.

curved surfaces of extremely thin, single-layered carbon frameworks as in ZTC [13,17,36,37]. In comparison, the NaOH-washing is a relatively safe route to oxygen functionalization of ZTC with retained pore orders (see the XRD peaks in Fig. 1). We investigated the chemical bonding of the beta-ZTC, Y-ZTC, and X-ZTC samples, using solid-state ^{13}C NMR and ATR-FTIR spectroscopies (Figs. 4, S4, and S5). The ^{13}C MAS NMR spectrum of the NaOH–HCl-washed beta-ZTC (beta-ZTC-NaOH) showed that the sp^2 framework of the ZTC was well retained after the NaOH–HCl washing treatments (120–150 ppm in Figs. 4a and S4) [13,38]. It was difficult to obtain quantitative information on oxygen-functional groups from the NMR spectra due to the low intensity of the peak at 180 ppm associated with carboxyl group [13]. Instead, the baseline-corrected ATR-FTIR spectra showed the presence of the oxygen-functional groups of the beta-ZTC (Figs. 4b and S5). Notably, there were increases in IR absorbance at 1,720 cm^{-1} corresponding to C=O stretching vibrations and 3,420 cm^{-1} to O–H [39], when NaOH was used for the template removal instead of HF (Fig. 4c). We attributed this result to the introduction of hydroxyl or carboxyl groups by the NaOH-based template washing. Moreover, the C=C stretching vibration regarding the conjugated system of C=C bonds was similarly observed at 1,580 cm^{-1} in both FTIR spectra [39], in accordance with the NMR result.

Organic functionalization is important for the development of

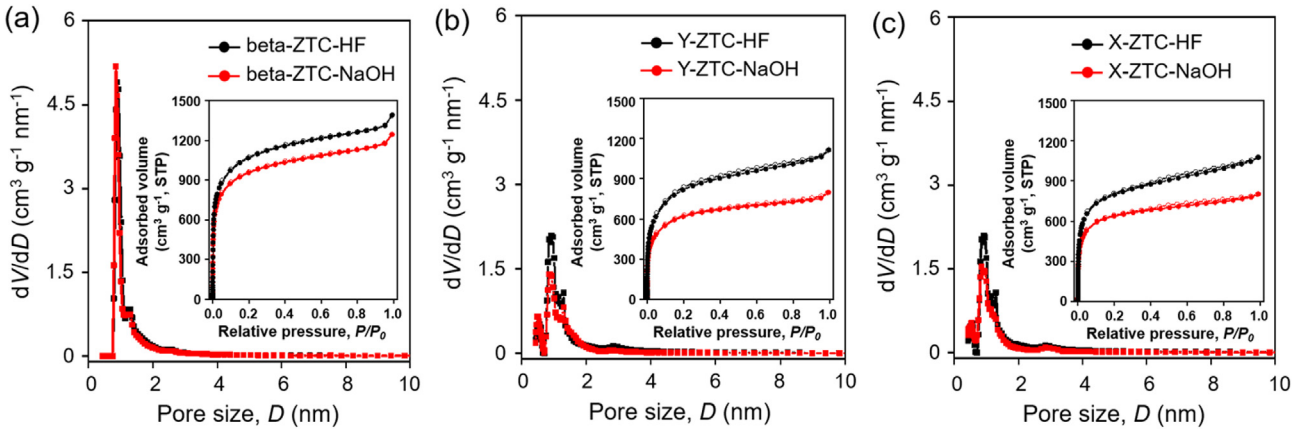

Fig. 3. QSDFT pore size distributions and corresponding Ar adsorption-desorption isotherms (insets) of (a) beta-ZTC, (b) Y-ZTC, and (c) X-ZTC samples obtained by NaOH- and HF-based template-washing methods (Entires 4, 6, 9 for NaOH-washing and 5, 8, 10 for HF-washing in Table 1). (A colour version of this figure can be viewed online.)

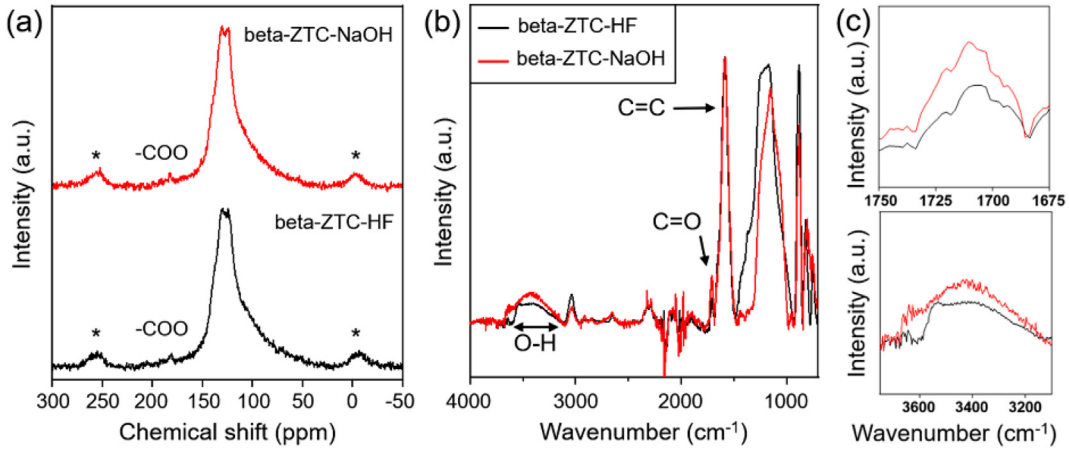

Fig. 4. Spectroscopic analysis of beta-ZTC samples obtained by NaOH- and HF-based template-washing methods. (a) ^{13}C MAS NMR and (b) baseline-corrected ATR-FTIR spectra of the beta-ZTC. (c) The FTIR spectra were expanded in the wavenumber regions of 1,675–1,750 cm^{-1} (top) and 3,100–3,750 cm^{-1} (bottom). Asterisks in the NMR spectra indicate spinning sidebands corresponding to a MAS rate of 13 kHz. (A colour version of this figure can be viewed online.)

future applicability of ZTC. Thus far, however, the functionalization of ZTC has only been reported in two limited cases: chemical grafting of a sulfonic acid group, and electrochemical bonding of an aniline moiety [40,41]. In the case of sulfonic acid, the functionalization was achieved via the reaction of chlorosulfuric acid with oxygen on the ZTC pore wall. The reacting oxygen-functional group might exist on the ZTC before the addition of chlorosulfuric acid, or more likely, it is generated *in situ* due to the oxidizing function of the chlorosulfuric acid. The functionalization resulted in a conspicuous decrease of pore orders and framework damage in the carbon [40]. On the other hand, in the case of aniline, the aromatic amine could be functionalized on the carbon more safely without structural damages [41], but the method requires a specialized electrochemical set up.

We speculated that the spontaneous generation of oxygen groups by NaOH, which is reported in this section, might provide a simpler and safer basis for organic functionalization in ZTC. To investigate this possibility, we grafted *N*,*N*-dimethylenediamine (DMEDA) groups through covalent bonding onto the beta-ZTC-NaOH sample, utilizing the one-pot carbodiimide-crosslinking reaction (see Section 1.2 in Supplementary data). After the functionalization treatment, the ZTC sample was analyzed by ^{13}C CP MAS NMR spectroscopy, elemental analysis, XRD and Ar adsorption (Fig. 5). The ^{13}C NMR spectrum of the amine-treated ZTC presented a chemical shift at 170 ppm (Fig. 5a), indicating that the amide bond was formed by the reaction of the carboxyl group with DMEDA. The presence of the amine group was checked by NMR peaks at around 30–40 ppm [42]. According to the elemental analysis, the nitrogen content of the amine-grafted beta-ZTC-NaOH (beta-ZTC-NaOH-DMEDA) was 2.4 mmol g^{-1}, which revealed that 1.4 times more amine group was grafted as compared with beta-ZTC–HF–DMEDA. In this manner, we confirmed that the increased oxygen content of the ZTC was useful for increasing the degree of amine functionalization. This was supported by the lower XRD peak intensity and micropore volume of beta-ZTC-NaOH-DMEDA (Fig. 5b and c), suggesting a higher amount of amine groups inside the carbon micropores. In addition, the amine-grafted beta-ZTC was tested as a catalyst in the Knoevenagel condensation between benzaldehyde and malononitrile at 333 K (see Section 1.3 in Supplementary data). The conversion of benzaldehyde at a reaction time of 6 h was 99% for beta-ZTC-NaOH-DMEDA, whereas it was only 31% for beta-ZTC–HF–DMEDA (Fig. 5d). These results indicated the higher amine group density of beta-ZTC-NaOH-DMEDA was useful for the catalytic application of ZTC. Comparatively, the benzaldehyde conversion of beta-ZTC-NaOH and beta-ZTC-HF was 0%. Moreover, the ZTC catalyst maintained the pore order after the reaction (Fig. S6), demonstrating the solvothermal stability of the carbon during the organic functionalization.

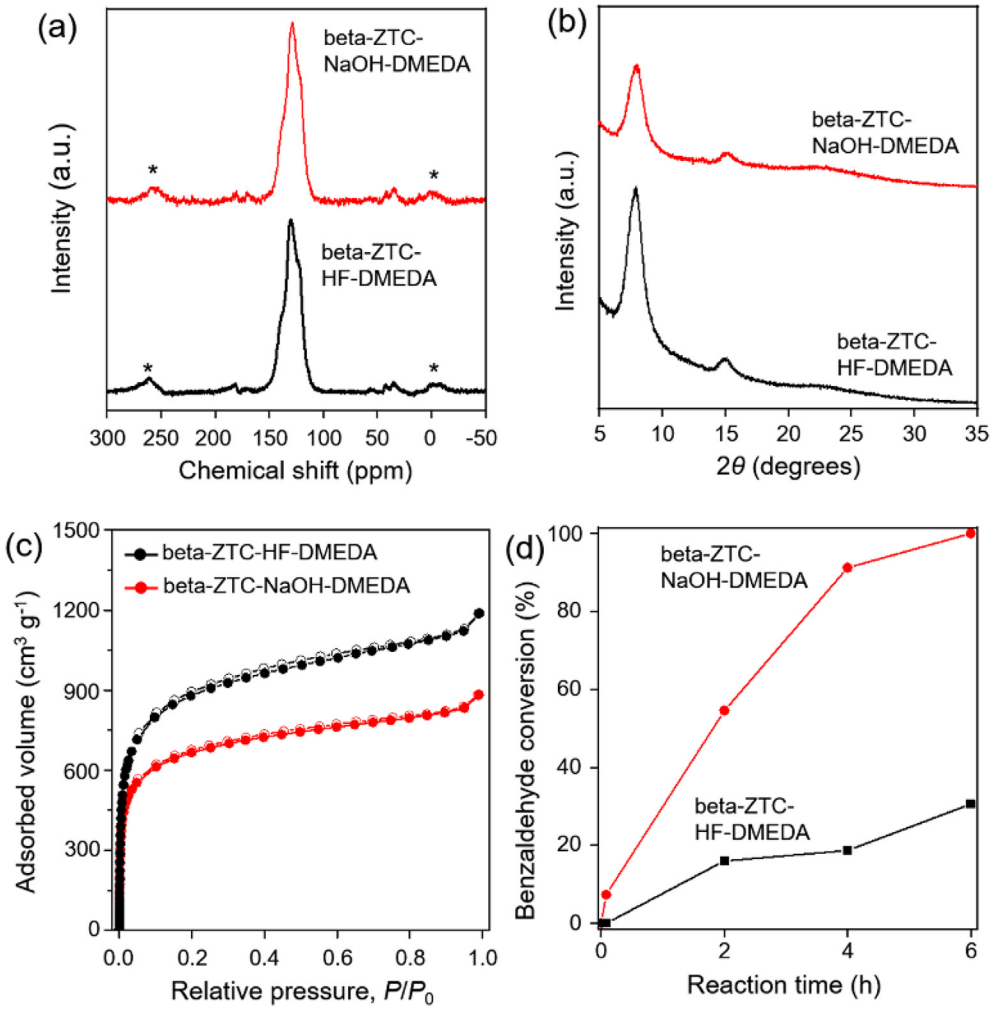

Fig. 5. Amine functionalization of beta-ZTC obtained by NaOH- or HF-based template removal. (a) ^{13}C CP MAS NMR spectra, (b) XRD patterns, (c) Ar adsorption-desorption isotherms, and (d) Knoevenagel condensation reaction of the amine-grafted beta-ZTC-HF (black) and beta-ZTC-NaOH (red). Asterisks in the NMR spectra indicate spinning sidebands. Conversion: amine-grafted beta-ZTC-NaOH (•, red), beta-ZTC-HF (■, black). Reaction conditions: benzaldehyde 5 mmol, malononitrile 7.5 mmol, catalyst 1 mol%, temperature = 333 K. (A colour version of this figure can be viewed online.)

3.4. *Effect of oxygen functionalities on conductivity and supercapacitance*

ZTC has been investigated as an electrode material for supercapacitor applications by taking the advantages of their high electrical conductivity and ordered microporous structure [8,13,43–46]. The oxygen-functional groups generated by the NaOH–HCl washing might have a negative impact on the electrical conductivity of the ZTC, while hydrophilic oxygen functionality can provide favorable interaction with an aqueous electrolyte [47]. In this regard, we measured the sheet resistance, local electrical conductance, and solution resistance (in non-aqueous and aqueous solutions) of the NaOH-washed ZTC for comparison with those of the HF-washed ZTC.

The sheet resistance of the NaOH-washed ZTC, measured by the four-point probe method, was higher than that of the HF-washed ZTC regardless of the zeolite framework types (Table S2). The local electrical conductance of the ZTC was determined by taking the slope of each *I–V* curve, which was taken from C-AFM measurements. Consistent with the sheet resistance results, the conductance of the NaOH-washed ZTC was lower compared with the HF-washed ZTC. We attributed this decrease in conductivity to the increase in the oxygen content, since these functional groups are known to disrupt an electrically conductive network [48]. Nonetheless, the conductance of the beta-ZTC-NaOH was still higher than that of mesoporous carbon (referred to as CMK-3) [49]. Furthermore, the EIS analyses of the ZTC was performed in both 1 M Et_4NBF_4/PC and 1 M K_2SO_4 (aq) solutions (Fig. S8). As determined by the EIS curves, the solution resistance of the NaOH-washed ZTC in the non-aqueous Et_4NBF_4/PC electrolyte was higher than that of the HF-washed ZTC (Table S2), while the trend was in a reverse order in the case of aqueous K_2SO_4 electrolyte. This result may be due to the combination of the decrease in the conductivity and the increase in the amount of the hydrophilic oxygen-functional groups.

The effect of the oxygen-functional groups on the electrochemical characteristics was examined by CV with two-electrode cells assembled with beta-ZTC electrodes in both the 1 M Et_4NBF_4/PC and 1 M K_2SO_4 (aq) electrolyte. In the case of the non-aqueous system, the stabilized CV curves of beta-ZTC in a potential range of 0–2.5 V showed a quasi-rectangular shape, indicating electrical double-layer capacitance (EDLC) together with pseudocapacitance as evidenced by faradaic responses associated with due to the oxidation/reduction of oxygen-functional groups (Figs. S9

and S10) [19]. The capacitive current of beta-ZTC-NaOH electrode was lower than that of beta-ZTC-HF due to the favorable interaction between the hydrophobic carbon framework and the non-aqueous electrolyte. In the case of the aqueous system, the CV curves of beta-ZTC also exhibited a quasi-rectangular shape, indicating the presence of the pseudocapacitance by broad faradaic responses associated with the oxidation/reduction of oxygen-functional groups (Fig. S10). Notably, the capacitive current of beta-ZTC-NaOH was higher than that of beta-ZTC-HF due to the increased oxygen content by the NaOH-washing, providing facilitated diffusion of the aqueous electrolyte through the micropore of the ZTC. The GCD curves of the electrochemical cells, measured at various current densities ranging from 0.1–10 A g^{-1}, presented a quasi-linear shape (Figs. S11 and 12). The GCD curves demonstrated both EDLC and pesudocapacitance regardless of the electrolytes [19], in a good agreement with the CV analysis. Derived from the discharge curves, the specific capacitances measured in the 1 M Et_4NBF_4/PC electrolyte were shown in Fig. 6b as a function of current density. At low current density (<1 A g^{-1}), the beta-ZTC-HF electrode showed higher capacitance of 93 F g^{-1} than that of beta-ZTC-NaOH (74 F g^{-1}). This 20% lower capacitance can mainly be ascribed to the difference in surface area of the ZTC, since the electrical charge storage in porous carbon materials has a positive correlation with their surface area [50,51]. As the current density was increased, the capacitance of the beta-ZTC-NaOH electrode decreased more rapidly compared with beta-ZTC-HF. The lower rate capability of beta-ZTC-NaOH can be attributed to the increased oxygen-functional groups, which impeded the electrolyte diffusion due to the decreased conductivity and the increased hydrophilicity [52].

To confirm that the decrease of conductivity and non-aqueous supercapacitor performance was due to the oxygen-functional groups on the ZTC, we attempted to reduce the oxygen content through H_2 gas treatment. The beta-ZTC-NaOH was treated by heating in H_2 at 723 K. After the H_2 treatment, the oxygen content of the carbon was reduced to 3.6 wt%, which was similar to that of the beta-ZTC-HF. The conductivity of the H_2-treated carbon (beta-ZTC-NaOH-[R]) was increased to a level comparable to that of beta-ZTC-HF (Fig. 6a). The non-aqueous supercapacitor performance was improved, and this result could be attributed to the increased conductivity. These results proved that the conductivity and electrochemical characteristics of the ZTC were changed by the increase and decrease of the oxygen contents. Given that the conductivity of beta-ZTC-NaOH and characteristics of the non-aqueous supercapacitor could be restored to a level similar to that of beta-ZTC-HF by the H_2 treatment, this phenomenon strongly resembles the reduction of graphene oxides for the restoration of the electrical properties [53,54].

Furthermore, the effect of oxygen functionalities in the ZTC on the aqueous supercapacitor performance was also investigated. Interestingly, we found that the increase in the oxygen functionalities dramatically improved the supercapacitive performance in the aqueous medium at higher current density. The specific capacitance was measured with the same procedure, except that an aqueous solution of 1 M K_2SO_4 was used as an electrolyte (Fig. 6c). At a low current density of 0.2 A g^{-1}, beta-ZTC-NaOH exhibited high specific capacitance of 390 F g^{-1} because of the high surface area, which was close to that of ZTC-HF (379 F g^{-1}). As the current density was increased, there was a significant drop in the capacitance in the case of beta-ZTC-HF, whereas beta-ZTC-NaOH showed a relatively small decrease in the capacitance with an increase in current density. In particular, beta-ZTC-NaOH exhibited high specific capacitance of 133 F g^{-1} at a high current density of 10 A g^{-1}, whereas beta-ZTC-HF showed only 44 F g^{-1} even at a lower current density of 4 A g^{-1}. The excellent aqueous supercapacitor performance of beta-ZTC-NaOH can be attributed to enhanced wettability of the micropore of the ZTC due to the presence of hydrophilic oxygen-functional groups. It is known that the micropores of carbon materials cannot be fully wetted in an aqueous solution, thereby impeding accessibility to the aqueous electrolyte [55]. The increase in the oxygen-functional groups in the beta-ZTC-NaOH not only improved the wettability, but also enhanced transportation of electrolyte ions through the ZTC micropores, which can promote facile diffusion for the electrochemical capacitive behavior [56,57]. To confirm the role of oxygen functionalities on the aqueous supercapacitor performance we reduce the oxygen in the beta-ZTC-NaOH through H_2 gas treatment. As the current density was increased, the specific capacitance of beta-ZTC-NaOH-[R] was significantly decreased in spite of the increase of conductivity (Fig. 6a and Table S2). In addition, when the X-ZTC and Y-ZTC samples obtained by the NaOH and HF-based washing were used as electrodes, the trends in electrochemical characteristics were similar to the case of the beta-ZTC sample in both electrolyte media (Fig. S13). We further conducted the charge/discharge cycling of the capacitor assembled with beta-ZTC-NaOH at a current density of 2 A g^{-1} for 10,000 cycles (Fig. S14), since the beta-ZTC-NaOH electrode showed the highest specific capacitance among all materials tested in this study. After 4000 cycles, the specific capacitance of

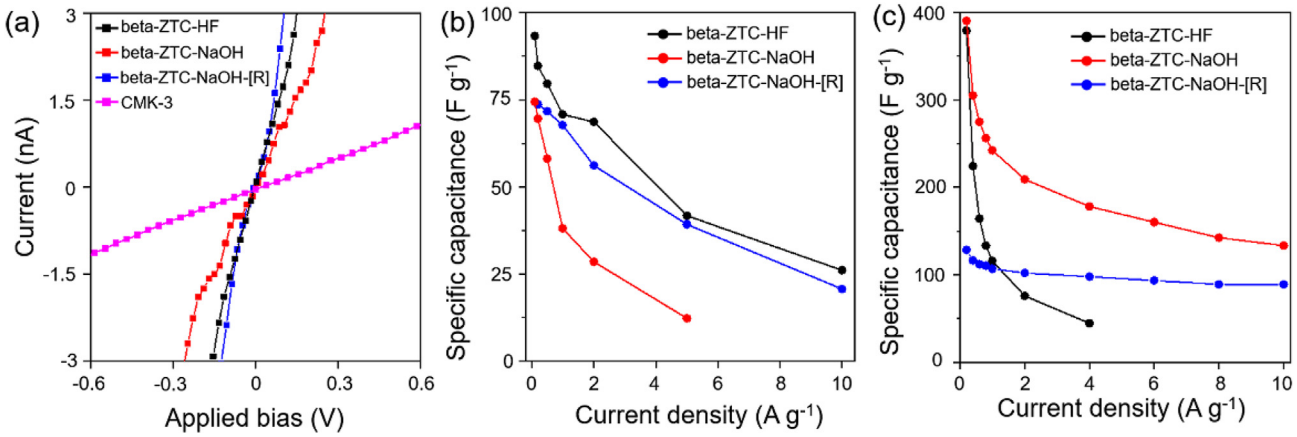

Fig. 6. Electrical conductance and supercapacitor performance of beta-ZTC samples obtained by NaOH- and HF-based template-washing methods and after H_2 treatment of beta-ZTC-NaOH. (a) *I–V* curves of the beta-ZTC. Specific capacitance of beta-ZTC electrodes in (b) 1 M Et_4NBF_4/PC and (c) aqueous 1 M K_2SO_4 electrolytes as a function of discharge current density. (A colour version of this figure can be viewed online.)

beta-ZTC-NaOH was decreased to 75 F g^{-1} and remained almost the same even after 10,000 cycles, revealing the electrochemical stability of the ZTC [19]. Overall, the increase in oxygen content by the NaOH-based zeolite-dissolution process significantly influenced the energy storage characteristics by decreasing the electrical conductivity and increasing the hydrophilicity of the ZTC. On the basis of these results, we suggest that the oxygen content of ZTC should be controlled for the desired energy storage applications.

4. Conclusions

In the present work, ordered microporous ZTC was successfully obtained by HF-free template removal using NaOH and HCl solutions, which was applicable to zeolite templates with various Si/Al ratios. The simple replacement of HF with NaOH of proper concentration could dissolve beta zeolite with high silica content, whereas an additional HCl treatment prior to the NaOH treatment was necessary in order to effectively eliminate aluminum in the case of FAU (Y and X) zeolites with low silica content. Compared with the HF-based washing, the ZTC obtained in this manner had higher oxygen content, which was due to oxygen-functional groups generated during the NaOH washing treatment. The increased oxygen functionalities could serve as a base for organic functionalization on the ZTC, as shown in the amine grafting for catalytic Knoevenagel condensation. Moreover, the increased oxygen content altered the electrical energy storage characteristics of the ZTC significantly, due to the decrease in electrical conductivity and the increase in hydrophilicity of the carbons. As a result, the supercapacitance in the non-aqueous Et_4NBF_4/PC electrolyte was low, but could be restored by reducing the oxygen functionalities through H_2 treatment under heating. On the other hand, in the case of an aqueous electrolyte system, hydrophilic oxygen-functional groups could facilitate the interaction with the aqueous K_2SO_4 solution, thereby markedly enhancing the retention of capacitance up to high current density. We believe that the NaOH-based template-washing methods offer a safer and environmentally friendlier route to ordered microporous carbons, which have high potential in various applications in electrical energy storage and heterogeneous catalysis.

Acknowledgment

The work was supported by IBS-R004-D1.

Appendix A. Supplementary data

Supplementary data to this article can be found online at https://doi.org/10.1016/j.carbon.2019.09.020.

References

[1] M.E. Davis, R.F. Lobo, Zeolite and molecular sieve synthesis, Chem. Mater. 4 (4) (1992) 756–768.
[2] C. Baerlocher, L.B. McCusker, D.H. Olson, Atlas of Zeolite Framework Types, sixth ed., Elsevier Science, 2007.
[3] P. Enzel, T. Bein, Poly(acrylonitrile) chains in zeolite channels: polymerization and pyrolysis, Chem. Mater. 4 (4) (1992) 819–824.
[4] T. Cordero, P. Thrower, L. Radovic, On the oxidation resistance of carbon-carbon composites obtained by chemical vapor infiltration of different carbon cloths, Carbon 30 (3) (1992) 365–374.
[5] T. Kyotani, T. Nagai, S. Inoue, A. Tomita, Formation of new type of porous carbon by carbonization in zeolite nanochannels, Chem. Mater. 9 (2) (1997) 609–615.
[6] S.A. Johnson, E.S. Brigham, P.J. Ollivier, T.E. Mallouk, Effect of micropore topology on the structure and properties of zeolite polymer replicas, Chem. Mater. 9 (11) (1997) 2448–2458.
[7] J. Rodriguez-Mirasol, T. Cordero, L.R. Radovic, J.J. Rodriguez, Structural and textural properties of pyrolytic carbon formed within a microporous zeolite template, Chem. Mater. 10 (2) (1998) 550–558.
[8] H. Nishihara, T. Kyotani, Zeolite-templated carbons – three-dimensional microporous graphene frameworks, Chem. Commun. 54 (45) (2018) 5648–5673.
[9] Z. Yang, Y. Xia, X. Sun, R. Mokaya, Preparation and hydrogen storage properties of zeolite-templated carbon materials nanocast via chemical vapor deposition: effect of the zeolite template and nitrogen doping, J. Phys. Chem. B 110 (37) (2006) 18424–18431.
[10] Z. Yang, Y. Xia, R. Mokaya, Enhanced hydrogen storage capacity of high surface area zeolite-like carbon materials, J. Am. Chem. Soc. 129 (6) (2007) 1673–1679.
[11] J.C. Bertolini, Hydrofluoric acid: a review of toxicity, J. Emerg. Med. 10 (2) (1992) 163–168.
[12] K. Kim, M. Choi, R. Ryoo, Ethanol-based synthesis of hierarchically porous carbon using nanocrystalline beta zeolite template for high-rate electrical double layer capacitor, Carbon 60 (2013) 175–185.
[13] K. Kim, T. Lee, Y. Kwon, Y. Seo, J. Song, J.K. Park, et al., Lanthanum-catalysed synthesis of microporous 3D graphene-like carbons in a zeolite template, Nature 535 (7610) (2016) 131–135.
[14] M.-C. Silaghi, C. Chizallet, P. Raybaud, Challenges on molecular aspects of dealumination and desilication of zeolites, Microporous Mesoporous Mater. 191 (2014) 82–96.
[15] G. Moon, A. Bähr, H. Tüysüz, Structural engineering of 3D carbon materials from transition metal Ion-exchanged Y zeolite templates, Chem. Mater. 30 (11) (2018) 3779–3788.
[16] L.D. Rollmann, E.W. Valyocsik, R.D. Shannon, Zeolite Molecular Sieves in Inorganic Syntheses, vol. 22, Wiley & Sons, New York, 1983.
[17] K. Kim, Y. Kwon, T. Lee, S.J. Cho, R. Ryoo, Facile large-scale synthesis of three-dimensional graphene-like ordered microporous carbon via ethylene carbonization in CaX zeolite template, Carbon 118 (2017) 517–523.
[18] F. Smits, Measurement of sheet resistivities with the four-point probe, Bell Syst Tech J 37 (3) (1958) 711–718.
[19] H. Lu, K. Kim, Y. Kwon, X. Sun, R. Ryoo, X.S. Zhao, Zeolite-templated nanoporous carbon for high-performance supercapacitors, J. Mater. Chem. 6 (2018) 10388–10394.
[20] E. Lippmaa, M. Maegi, A. Samoson, M. Tarmak, G. Engelhardt, Investigation of the structure of zeolites by solid-state high-resolution silicon-29 NMR spectroscopy, J. Am. Chem. Soc. 103 (17) (1981) 4992–4996.
[21] R.K. Iler, The Chemistry of Silica: Solubility, Polymerization, Colloid and Surface Properties and Biochemistry of Silica, Wiley, New York, 1979.
[22] J.C. Groen, J.A. Moulijn, J. Pérez-Ramírez, Desilication: on the controlled generation of mesoporosity in MFI zeolites, J. Mater. Chem. 16 (22) (2006) 2121–2131.
[23] H.K. Beyer, Dealumination techniques for zeolites, in: H.G. Karge, Weitkamp Jens (Eds.), Post-synthesis Modification I, Springer, 2002.
[24] D. Verboekend, G. Vilé, J. Pérez-Ramírez, Hierarchical Y and USY zeolites designed by post-synthetic strategies, Adv. Funct. Mater. 22 (5) (2012) 916–928.
[25] Y. Li, X. Wang, T. Thersleff, G. Svensson, N. Hedin, Silicoaluminophosphate (SAPO)-templated activated carbons, ACS Omega 4 (6) (2019) 9889–9895.
[26] J.T. Kim, M.C. Kim, Y. Okamoto, T. Imanaka, Acid attack theory of dealumination in cation-exchanged faujasite, J. Catal. 115 (2) (1989) 319–325.
[27] Z.X. Ma, T. Kyotani, A. Tomita, Preparation of a high surface area microporous carbon having the structural regularity of Y zeolite, Chem. Commun. 0 (23) (2000) 2365–2366.
[28] H.-L. Chiang, C. Huang, P. Chiang, The surface characteristics of activated carbon as affected by ozone and alkaline treatment, Chemosphere 47 (3) (2002) 257–265.
[29] J.P. Chen, S. Wu, Acid/base-treated activated carbons: characterization of functional groups and metal adsorptive properties, Langmuir 20 (6) (2004) 2233–2242.
[30] C.-L. Lin, C.-C. Wang, Enhancement of electroactivity of platinum–tungsten trioxide nanocomposites with NaOH-treated carbon support toward methanol oxidation reaction, Appl. Energy 164 (2016) 1043–1051.
[31] S. Biniak, G. Szymański, J. Siedlewski, A. Świątkowski, The characterization of activated carbons with oxygen and nitrogen surface groups, Carbon 35 (12) (1997), 1799-10.
[32] C.G. Salzmann, S.A. Llewellyn, G. Tobias, M.A. Ward, Y. Huh, M.L. Green, The role of carboxylated carbonaceous fragments in the functionalization and spectroscopy of a single-walled carbon-nanotube material, Adv. Mater. 19 (6) (2007) 883–887.
[33] X. Fan, W. Peng, Y. Li, X. Li, S. Wang, G. Zhang, et al., Deoxygenation of exfoliated graphite oxide under alkaline conditions: a green route to graphene preparation, Adv. Mater. 20 (23) (2008) 4490–4493.
[34] A.-N.A. El-Hendawy, Influence of HNO_3 oxidation on the structure and adsorptive properties of corncob-based activated carbon, Carbon 41 (4) (2003) 713–722.
[35] A.-H. Lu, W.-C. Li, N. Muratova, B. Spliethoff, F. Schüth, Evidence for C–C bond cleavage by H_2O_2 in a mesoporous CMK-5 type carbon at room temperature, Chem. Commun. 0 (41) (2005) 5184–5186.
[36] H. Nishihara, Q.H. Yang, P.X. Hou, M. Unno, S. Yamauchi, R. Saito, et al., A possible buckybowl-like structure of zeolite templated carbon, Carbon 47 (5) (2009) 1220–1230.
[37] H. Nishihara, H. Fujimoto, H. Itoi, K. Nomura, H. Tanaka, M.T. Miyahara, et al., Graphene-based ordered framework with a diverse range of carbon polygons formed in zeolite nanochannels, Carbon 129 (2018) 854–862.

[38] A.M. Panich, V.Y. Osipov, H. Nishihara, T. Kyotani, Nuclear magnetic resonance study of zeolite-templated carbon, Synth. Met. 221 (2016) 149–152.
[39] D.C. Marcano, D.V. Kosynkin, J.M. Berlin, A. Sinitskii, Z. Sun, A. Slesarev, et al., Improved synthesis of graphene oxide, ACS Nano 4 (8) (2010) 4806–4814.
[40] K. Fukuhara, K. Nakajima, M. Kitano, S. Hayashi, M. Hara, Synthesis and acid catalysis of zeolite-templated microporous carbons with SO_3H groups, Phys. Chem. Chem. Phys. 15 (23) (2013) 9343–9350.
[41] C. González-Gaitán, R. Ruiz-Rosas, H. Nishihara, T. Kyotani, E. Morallón, D. Cazorla-Amorós, Successful functionalization of superporous zeolite templated carbon using aminobenzene acids and electrochemical methods, Carbon 99 (2016) 157–166.
[42] E.P. Dillon, C.A. Crouse, A.R. Barron, Synthesis, characterization, and carbon dioxide adsorption of covalently attached polyethyleneimine-functionalized single-wall carbon nanotubes, ACS Nano 2 (1) (2008) 156–164.
[43] H. Nishihara, T. Kyotani, Templated nanocarbons for energy storage, Adv. Mater. 24 (33) (2012) 4473–4498.
[44] W. Gu, G. Yushin, Review of nanostructured carbon materials for electrochemical capacitor applications: advantages and limitations of activated carbon, carbide-derived carbon, zeolite-templated carbon, carbon aerogels, carbon nanotubes, onion-like carbon, and graphene, WIREs Energy Environ 3 (5) (2014) 424–473.
[45] H. Lee, K. Kim, S.-H. Kang, Y. Kwon, J.H. Kim, Y.-K. Kwon, et al., Extremely high electrical conductance of microporous 3D graphene-like zeolite-templated carbon framework, Sci. Rep. 7 (1) (2017) 11460.
[46] C. Young, T. Park, J.W. Yi, J. Kim, M.S.A. Hossain, Y.V. Kaneti, et al., Advanced functional carbons and their hybrid nanoarchitectures towards supercapacitor applications, ChemSusChem 11 (20) (2018) 3546–3558.
[47] Y.-T. Kim, T. Mitani, Competitive effect of carbon nanotubes oxidation on aqueous EDLC Performance: balancing hydrophilicity and conductivity, J. Power Sources 158 (2) (2006) 1517–1522.
[48] D.R. Dreyer, S. Park, C.W. Bielawski, R.S. Ruoff, The chemistry of graphene oxide, Chem. Soc. Rev. 39 (1) (2008) 228–240.
[49] S. Jun, S.H. Joo, R. Ryoo, M. Kruk, M. Jaroniec, Z. Liu, et al., Synthesis of new, nanoporous carbon with hexagonally ordered mesostructure, J. Am. Chem. Soc. 122 (43) (2000) 10712–10713.
[50] D. Lozano-Castello, D. Cazorla-Amorós, A. Linares-Solano, S. Shiraishi, H. Kurihara, A. Oya, Influence of pore structure and surface chemistry on electric double layer capacitance in non-aqueous electrolyte, Carbon 41 (9) (2003) 1765–1775.
[51] L.L. Zhang, X.S. Zhao, Carbon-based materials as supercapacitor electrodes, Chem. Soc. Rev. 38 (9) (2009) 2520–2531.
[52] L. Zhang, G. Shi, Preparation of highly conductive graphene hydrogels for fabricating supercapacitors with high rate capability, J. Phys. Chem. C 115 (34) (2011) 17206–17212.
[53] D.V. Kosynkin, A.L. Higginbotham, A. Sinitskii, J.R. Lomeda, A. Dimiev, B.K. Price, et al., Longitudinal unzipping of carbon nanotubes to form graphene nanoribbons, Nature 458 (7240) (2009) 872–876.
[54] S. Pei, H.-M. Cheng, The reduction of graphene oxide, Carbon 50 (9) (2012) 3210–3228.
[55] C.-T. Hsieh, H. Teng, Influence of oxygen treatment on electric double-layer capacitance of activated carbon fabrics, Carbon 40 (5) (2002) 667–674.
[56] C.O. Ania, V. Khomenko, E. Raymundo-Piñero, J.B. Parra, F. Béguin, The large electrochemical capacitance of microporous doped carbon obtained by using a zeolite template, Adv. Funct. Mater. 17 (11) (2007) 1828–1836.
[57] M. Vujković, D. Bajuk-Bogdanović, L. Matović, M. Stojmenović, S. Mentus, Mild electrochemical oxidation of zeolite templated carbon in acidic solutions, as a way to boost its charge storage properties in alkaline solutions, Carbon 138 (2018) 369–378.